Folding Mechanism of the α-Subunit of Tryptophan Synthase, an α/β Barrel Protein: Global Analysis Highlights the Interconversion of Multiple Native, Intermediate, and Unfolded Forms through Parallel Channels†

Osman Bilsel, Jill A. Zitzewitz, Katherine E. Bowers, and C. Robert Matthews*

Department of Chemistry and Center for Biomolecular Structure and Function, The Pennsylvania State University, University Park, Pennsylvania 16802

Received October 2, 1998; Revised Manuscript Received November 16, 1998

ABSTRACT: A variety of techniques have been used to investigate the urea-induced kinetic folding mechanism of the α-subunit of tryptophan synthase from *Escherichia coli*. A distinctive property of this 29 kDa α/β barrel protein is the presence of two stable equilibrium intermediates, populated at approximately 3 and 5 M urea. The refolding process displays multiple kinetic phases whose lifetimes span the submillisecond to greater than 100 s time scale; unfolding studies yield two relaxation times on the order of 10−100 s. In an effort to understand the populations and structural properties of both the stable and transient intermediates, stopped-flow, manual-mixing, and equilibrium circular dichroism data were globally fit to various kinetic models. Refolding and unfolding experiments from various initial urea concentrations as well as forward and reverse double-jump experiments were critical for model discrimination. The simplest kinetic model that is consistent with all of the available data involves four slowly interconverting unfolded forms that collapse within 5 ms to a marginally stable intermediate with significant secondary structure. This early intermediate is an off-pathway species that must unfold to populate a set of four on-pathway intermediates that correspond to the 3 M urea equilibrium intermediate. Reequilibrations among these conformers act as rate-limiting steps in folding for a majority of the population. A fraction of the native conformation appears in less than 1 s at 25 °C, demonstrating that even large proteins can rapidly traverse a complex energy surface.

The folding reactions of many proteins are complex, involving transient, partially folded forms. An understanding of the structures and energies of these intermediates is essential in elucidating the mechanism by which the one-dimensional sequence information is converted into three-dimensional structure (*1*−*4*). However, their milliseconds-to-seconds lifetimes impede a detailed characterization of these partially folded forms.

One approach toward overcoming this problem is to identify equilibrium conditions under which similar, if not identical, species are significantly populated. Molten globules, which are stable under extreme solvent conditions such as low pH, high salt, or moderate denaturant conditions, are the classic example of partially folded forms that have been thoroughly characterized under equilibrium conditions (*5*, *6*). However, only for a few proteins, including apomyoglobin (*7*), α-lactalbumin (*8*), and RNase H (*9*), has a direct correspondence between these molten globule forms and transient folding intermediates been demonstrated. The native state hydrogen exchange experiment has also been used to detect partially unfolded conformations (*10*−*13*); however, the role of some of these species in the folding mechanisms remains unclear. Protein fragments can also serve as models for protein folding intermediates (*14*−*16*). The challenges with fragmentation studies, however, include identifying soluble sequences with significant stability and correlating fragment equilibrium and kinetic properties with those of the full-length protein. Although these alternative approaches have provided important insights, studies of the folding mechanisms of full-length proteins remain essential.

For proteins whose folding reactions exhibit complex kinetic responses, it becomes necessary to use a multifaceted approach that combines a variety of equilibrium and kinetic methods for the characterization of partially folded intermediates (*17*, *18*). A suitable candidate for these type of studies is the α-subunit of tryptophan synthase (αTS[1]), a 29 kDa protein which is a member of the α/β barrel class of proteins (*19*). A striking property of αTS is the significant population of at least two stable, partially folded intermediates at low to moderate urea concentrations (*20*, *21*). Equilibrium intermediates have also been observed in at least two other α/β barrel proteins, phosphoribosylanthranilate isomerase

† This work was supported by the National Institutes of Health through Grant GM23303 to C.R.M. Partial support was also provided by NIH Postdoctoral Fellowship Awards GM17814 to O.B. and GM14954 to J.A.Z.

* To whom correspondence should be addressed.

[1] Abbreviations: αTS, the α-subunit of tryptophan synthase from *Escherichia coli*; CD, circular dichroism; DTE, dithioerythritol; Gdn-HCl, guanidine hydrochloride; I1, equilibrium intermediate of αTS populated in 3 M urea; I2, equilibrium intermediate of αTS populated in 5 M urea; I_{BP}, kinetic intermediate of αTS populated within the stopped-flow burst phase; K_2EDTA, ethylenediaminetetraacetic acid, dipotassium salt; N, native state; SDS, sodium dodecyl sulfate; SVD, singular value decomposition; U, unfolded state.

10.1021/bi982365q CCC: $18.00
Published on Web 12/22/1998

(*22*, *23*) and indole-3-glycerol phosphate synthase (*24*), suggesting that this may be a common property of this class of proteins. In the case of αTS, this feature can be advantageous in the determination of the folding mechanism underlying the complex kinetics. Additionally, a more thorough characterization of transient intermediates is possible if they can be directly correlated to equilibrium intermediates.

Earlier studies on αTS uncovered several qualitative features of the folding mechanism. These features include a single unfolding phase, a slow isomerization reaction, and a single rate-limiting step leading to a single native conformation. On the basis of these results, several folding models have been previously proposed (*25*−*27*). More recent kinetic data in which multiple unfolding phases and a refolding burst phase are observed (*28*, *29*) indicate that the kinetic mechanism must be more complex.

The purpose of the present work is to provide a quantitative description of the folding kinetics of αTS. To this end, a wide variety of kinetic refolding and unfolding data were acquired by circular dichroism spectroscopy on the millisecond to greater than 100 s time scale. In addition, the presence of stable equilibrium intermediates permits refolding, unfolding, and various double-jump experiments from/to a greater number of conditions than is possible with a simple two-state equilibrium system. By integrating the results of these double-jump experiments with a global analysis of the refolding and unfolding data, it is possible to discard incorrect models and to determine the stabilities of the partially folded forms that appear during the folding of αTS.

MATERIALS AND METHODS

Materials. All materials were reagent grade with the exception of ultrapure urea, which was purchased from ICN Biomedicals, Inc. (Aurora, OH). For some unfolding experiments, the ultrapure urea was further purified by recrystallization in water. This step increased transmittance in the far-UV region, presumably by reducing the concentration of absorbing impurities such as cyanate. The increased transmittance at 222 nm yielded noticeable improvements (>3×) in the signal-to-noise ratio for CD experiments at high urea concentrations.

Protein Expression and Purification. αTS was isolated from the *E. coli* host W3110 (ΔtonB-trp)BA17*his*$^-$ containing the plasmid pBN55. The protein was purified from the soluble extract following a modified procedure of Kirschner et al. (*30*). The protein was extracted from the cells by sonication and the supernatant was applied to a DEAE-52 (Whatman) column equilibrated at 4 °C with 10 mM potassium phosphate, pH 7.8, 2 mM K_2EDTA, and 2 mM DTE. The protein was eluted by a stepwise increase of the K_2EDTA concentration in the buffer to 4 mM. Fractions containing purified protein were confirmed by the presence of a single band on a 15% SDS polyacrylamide gel. Protein was stored at 4 °C as an 80% ammonium sulfate precipitate and dialyzed before use against the standard buffer used for all folding experiments (10 mM potassium phosphate, pH 7.8, 0.2 mM K_2EDTA, and 1 mM β-mercaptoethanol). Protein concentration was determined from the UV absorbance at 278 nm, using an extinction coefficient of 12 600 M^{-1} cm^{-1} (*31*).

Equilibrium Unfolding Experiments. The samples used to determine the thermodynamic properties of the urea denaturation of αTS were prepared with a Hamilton 540B automatic titrator interfaced to an Aviv 62ADS spectropolarimeter. Stocks of 3 μM αTS in buffer and in approximately 9 M recrystallized urea-containing buffer were mixed in the desired amounts to vary the final urea concentration from 0 to 8 M urea. A computer running in-house software was used to control both the Aviv 62ADS spectrometer and the automatic titrator. Data were collected for 100 s at 222 nm using a path length of 1.0 cm and bandwidth of 2.5 nm. Equilibration times between additions always exceeded 3× the observed relaxation times at the same urea concentration. Equivalent results were obtained by manually preparing the samples and equilibrating for >1 h prior to data collection.

Kinetic Unfolding and Refolding Experiments. Stopped-flow CD refolding experiments were performed on an Aviv model 62DS CD spectrophotometer interfaced with a Biologic SFM-3 stopped-flow drive train. The temperature was maintained at 25 °C using a water bath. The cell path length was 2.0 mm, and the dead-time for mixing was 5 ms (*32*).

CD manual-mixing and double-jump experiments were performed on an Aviv model 62DS or 62ADS CD spectrophotometer, equipped with a thermoelectric cell holder. These experiments were performed using a 1 cm path length cell and an averaging time of 1 s. The dead-time for manual-mixing experiments, i.e., the time required to add the protein sample to the stirring urea/buffer solution and start the instrument, was 2−4 s. To account for the instrument response time, an additional 4−6 s of data were omitted.

Unfolding jumps were performed by a 20-fold dilution from 0 M urea to various final concentrations of urea (2−7 M). Similarly, manual-mixing refolding jumps were performed by a 1:20 dilution from 8 M to various final concentrations of urea (0.4−5 M). For stopped-flow CD experiments, folding was intitiated by a 1:10 dilution from 6 M urea to a final concentration ranging from 0.6 to 3.6 M urea. Unfolding jumps from various initial concentrations (1.4−5.6 M) to a final concentration of 6 M urea were also carried out as well as refolding jumps starting from various initial concentrations of urea (2.4−6 M) to a final concentration of 0.6 M urea. Samples were allowed to equilibrate for >1 h prior to initiation of all refolding/unfolding kinetics. The initial and final urea concentration in all experiments were determined from the index of refraction (*33*). The final protein concentration was typically 3−5 μM for all experiments.

For double-jump refolding assays, protein in buffer was unfolded to 8 M urea. After various delay times, the protein was refolded by dilution with buffer to a final concentration of 0.4 M urea. For the double-jump unfolding assays, protein was unfolded in 5 or 8 M urea and allowed to equilibrate for >1 h. The unfolded protein solution was then diluted with buffer to a final urea concentration of 0.25 M. After various delay times, the protein was unfolded by dilution to either 2.4 or 6 M urea.

Data Analysis. Equilibrium data were fit to a three-state model as described previously (*34*). The free energy changes were assumed to depend linearly on the denaturant concentration (*35*).

The kinetic data obtained from unfolding and refolding experiments to varying final urea concentrations were fit by

two different methods. First, a phenomenological description of the data was obtained by fitting kinetic traces at a particular urea concentration to the sum of a minimum number of statistically significant exponential functions and a constant (*36*). The second method was directed toward the elucidation of a kinetic model and estimation of microscopic rate constants directly from the raw kinetic data. This method utilized a global approach (*37*) in which both refolding and unfolding kinetic traces at various final urea concentrations were fit simultaneously to a particular kinetic model (*38*). Specifically, the time dependence of the concentration of species i at a particular urea concentration, $c_i(t,\text{urea})$, can be described by the solution of the eigenvalue equation (*39*)

$$\frac{dc_i(t)}{dt} = -\sum_{j=1,n;j\neq i} k_{ij}c_i(t) + \sum_{j=1,n;j\neq i} k_{ji}c_j(t) \qquad (1)$$

where k_{ij} represents the microscopic rate constant for conversion of species i to j and n is the total number of species. The simultaneous fitting of all of the refolding and unfolding data was accomplished by further parametrizing k_{ij} as a function of the urea concentration by assuming a linear dependence of the activation free energy on urea concentration (*40*)

$$k_{ij} = k_{ijo}e^{-m_{ij}[\text{urea}]/RT} \qquad (2)$$

Thus, the entire kinetic system may be described by the rate constants in the absence of urea (k_{ijo}), their dependence on urea (m_{ij}), and the optical properties of the intermediates. These parameters were then optimized using an in-house global nonlinear least-squares package (Savuka, version 5.12). All nonlinear fits were performed using the Marquardt−Levenburg algorithm (*41*). The initial conditions for eq 1 were obtained from the steady-state solution to eq 1 at the initial urea concentration.

Some optimizations were also performed simultaneously on kinetic and equilibrium data. The equilibrium data utilized in this manner permitted more accurate determinations of the native and unfolded baselines. Typically, these baseline parameters are known quantities from equilibrium studies and were kept fixed during optimizations. Protein concentration was treated as an adjustable parameter because discrepancies on the order of a few percent between kinetic traces gave rise to significant penalties along the global χ^2 surface. Because this is a unimolecular kinetic system, the protein concentration parameter functions as a local scaling factor which does not affect the kinetics.

Typically, the optical properties of the intermediates in a multistate equilibrium denaturation curve are described relative to the baselines of the native and unfolded species. The "Z-value" is defined as $Z = (Y_I - Y_N)/(Y_U - Y_N)$, where Y_N, Y_I, and Y_U depend on the urea concentration and refer to the optical properties of the native, intermediate, and unfolded forms, respectively (*36*). This approximation was also used to describe the optical properties of the intermediates in the kinetic models.

This type of parametrization and analysis offers the possibility to overdetermine the system and significantly enhance the ability to discriminate between competing kinetic models. However, for some kinetic schemes, such as when parallel folding channels are present, the complexity of the system can render it indeterminate (*39*). In these cases, the results of additional experiments (e.g., double-jump assays and refolding/unfolding from varying initial conditions) were utilized to narrow the search space of some parameters and are introduced where applicable.

Refolding and unfolding kinetic data starting from different initial conditions and ending in a single-jump to the same final condition were fit by two different methods. The first method involved directly fitting all of the unfolding or refolding kinetics to a sum of exponentials with the time constants linked in a global analysis (*37*). Because the final conditions are the same, the kinetics should differ only in the amplitudes of the various phases. This type of analysis yields amplitudes at or near both the native and unfolded baselines, where independent determination of the time constants is hindered by very small changes in signal amplitude.

The second method involved decomposing the data matrix of ellipticity measurements along the two independent experimental axes, initial urea concentration and refolding or unfolding time, using SVD (*42*). The SVD algorithm, which has been applied to a variety of experimental data (*43*−*47*), is suitable because the final urea concentrations, and thus the time constants, are the same. Therefore, the data matrix is represented as

$$\mathbf{A} = \mathbf{U}\cdot\mathbf{W}\cdot\mathbf{V}^T \qquad (3)$$

where the basis vectors of the matrix **U** represent the dependence of all of the amplitudes on the initial urea concentration, the basis vectors of the matrix **V** represent the kinetics at the final urea concentration, and the diagonals of the matrix **W** represent the weights of each of the basis vectors. The significant basis vectors of **V** were fit to a sum of the minimum number of statistically significant exponentials, which was determined by considering the weights of the basis vectors and their autocorrelations. Three exponential functions were used for refolding, and two were used for unfolding. The dependences of the refolding or unfolding amplitudes on initial urea concentration were then obtained by reconstructing the data matrix by matrix multiplication and propagating the fit parameters accordingly. These amplitudes were then fit to a two- or three-state unimolecular equilibrium unfolding model. Both methods gave identical results.

The double-jump refolding and unfolding kinetic assays were also analyzed with both methods. In either case, the data matrix was comprised of ellipticity measurements under the same final conditions along two independent experimental axes, the delay time and the refolding or unfolding time. For the exponential terms describing the refolding or unfolding time dependence, the time constants were linked and separate amplitudes were obtained for each delay time. The refolding or unfolding amplitudes as a function of delay time were, in turn, fit to a sum of exponential functions.

RESULTS AND ANALYSIS

To elucidate the folding mechanism for αTS, three basic types of kinetic experiments were performed. Traditional kinetic experiments, involving unfolding from the native state or refolding from the unfolded state, were used to probe the mechanism under a variety of final conditions. Double-jump

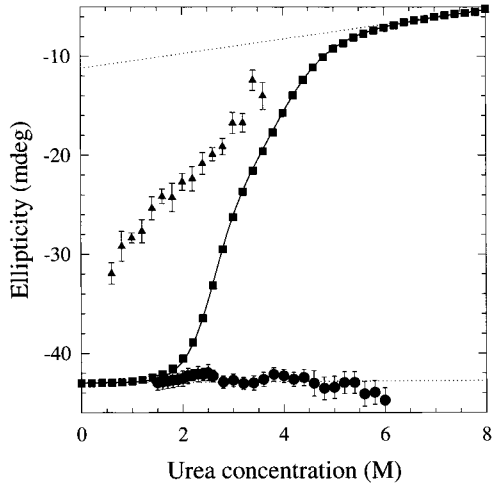

FIGURE 1: Equilibrium unfolding curve (squares) for αTS monitored by CD at 222 nm. The solid line shows the calculated curve using the kinetic parameters from Table 1. The burst-phase amplitude obtained from stopped-flow refolding kinetic jumps from 6 M to various final urea concentrations (triangles), and the unfolding burst-phase amplitude from manual-mixing jumps from 0 M urea (circles) are also shown. The dotted lines indicate the fitted baselines for the native and unfolded forms. Conditions: 3−5 μM αTS, 10 mM potassium phosphate, pH 7.8, 0.2 mM K_2EDTA, and 1 mM β-mercaptoethanol at 25 °C. The data have been normalized to an αTS concentration of 1 μM.

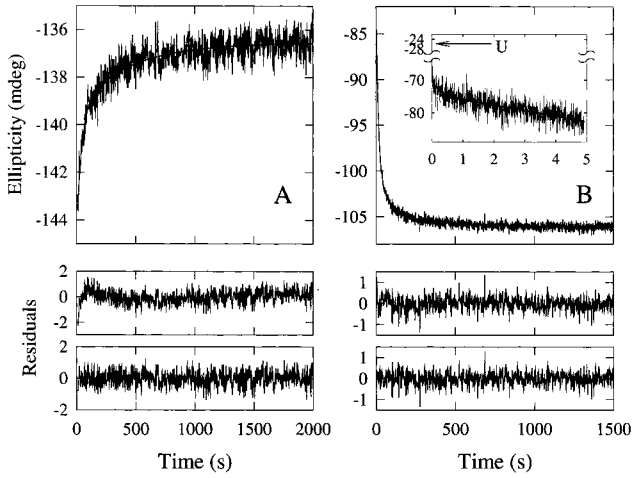

FIGURE 2: (A) Unfolding kinetic trace from 0 to 2.2 M urea as monitored by manual-mixing CD at a protein concentration of 3 μM. Under these final conditions the equilibrium intermediate is significantly populated and only a small fraction of the protein is unfolded. The line represents the fit of the data to two exponentials with time constants of 104 ± 5 and 600 ± 64 s. The residuals for fits to 1 and 2 exponentials, respectively, are also shown. (B) Refolding kinetic trace from 6 to 0.6 M urea as monitored by manual-mixing or stopped-flow (inset) CD; the initial ellipticity of the unfolded form is indicated by the arrow in the inset. The residual plots of the two and three exponential fits of the manual-mixing data are also shown. The concentration of αTS is 2.5 μM for the manual-mixing trace and 5 μM for the stopped-flow kinetics. For clarity, the stopped-flow CD data in the inset has been scaled to the longer time manual-mixing data to account for differences in protein concentration and cell path length. Other conditions are described in the caption to Figure 1. The combined manual-mixing and stopped-flow kinetic traces are best described by a total of four exponentials with relaxation times of 500 ms, 10 s, 40 s, and ~300 s.

experiments (N → U → delay time → N and U → N → delay time → U) were used to monitor the time dependence of the population of multiple native, stable intermediate, and unfolded forms. Last, kinetic experiments from varying initial to constant final conditions were used to probe the role of preexisting stable intermediates in the mechanism. Circular dichroism spectroscopy was used to monitor the folding reaction because the amplitudes could be readily quantified and correlated between experiments. CD also offered the advantage of accurate long-time data collection; photobleaching precluded the use of fluorescence spectroscopy.

Equilibrium Unfolding. The equilibrium unfolding of αTS in urea, as monitored by CD, is shown in Figure 1. The nearly constant signal below 2 M urea indicates that the native conformation is the primary species under these conditions. The sigmoidal decrease in ellipticity between 2 and 6 M urea is indicative of a global unfolding reaction that dramatically disrupts the secondary structure of αTS. The inflection in the unfolding transition near 3 M urea reveals the presence of the equilibrium intermediate, I1 (*20*).

A second equilibrium intermediate, detected by the presence of a slow-exchanging His Cϵ peak in the ^{1}H NMR spectrum, was shown to be maximally populated at 5 M urea (*21*). This intermediate, I2, is nearly indistinguishable from U by CD under the conditions of these experiments. Therefore, I2 and U effectively behave as a single thermodynamic state, I2/U. Above 6 M urea, the linear decrease in CD signal indicates that the unfolded form is the principal thermodynamic state.

The data were fit to a three-state equilibrium model, yielding free energies under standard state conditions of 5.3 ± 0.2 kcal mol^{-1} for the N ⇄ I1 transition and 4.8 ± 0.2 kcal mol^{-1} for the I1 ⇄ I2/U transition, with associated *m* values of 2.0 ± 0.1 and 1.2 ± 0.1 kcal mol^{-1} M^{-1}, respectively, and a *Z* value of 0.54. The midpoints of the N ⇄ I1 and I1 ⇄ I2/U unfolding transitions are 2.7 and 4.2 M urea, respectively. Additional experiments that rely on Tyr fluorescence (P. G. Gualfetti, O.B., and C.R.M., unpublished results) confirm that these thermodynamic parameters correspond closely to the N ⇄ I1 and I1 ⇄ I2 transitions in the four-state model.

Unfolding Kinetics to Varying Final Urea Concentrations (0 → x M Urea). The kinetics of unfolding monitored by manual-mixing CD spectroscopy are shown in Figure 2A. A distinctive feature of the unfolding data is the presence of a second minor, slower kinetic phase. Although previous studies of the unfolding of αTS in urea only detected a single phase (*20*), the observation of an additional unfolding phase is attributable primarily to the increased signal-to-noise obtained with recrystallized urea. A second, relatively minor, kinetic phase has previously been reported for αTS under strongly unfolding conditions in Gdn-HCl (>3 M) (*28*). However, an additional unfolding phase was not observed at Gdn-HCl concentrations below or near the midpoint of the first equilibrium unfolding transition as is seen with urea.

The unfolding time constants as a function of the final urea concentration are shown in Figure 3. The faster unfolding phase exhibits a maximum near 3 M urea, and the slower phase is nearly denaturant-independent in the same region. The time constant for the fast phase decreases exponentially at both higher and lower concentrations of urea, while that for the slower phase only decreases at higher urea concentration. The dominant faster unfolding phase is similar to the single phase reported previously (*27*). Although only a single phase is reported between 4 and 6 M urea in Figure

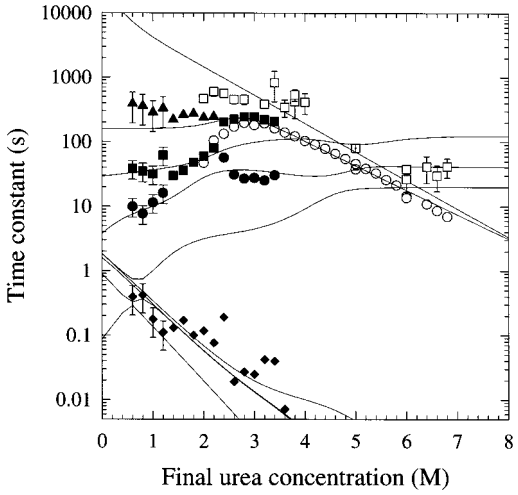

FIGURE 3: Unfolding (open symbols) and refolding (closed symbols) relaxation times obtained from exponential fits of the unfolding and refolding data as a function of final urea concentration. The number of statistically significant exponentials used in fitting the data at a particular urea concentration are illustrated by the different symbols. Urea dependences of the relaxation times based on the time constants (i.e., eigenvalues) were calculated using the kinetic parameters obtained from the global fit and are represented as lines. The calculated time constants reproduce the four kinetic phases (diamonds, 500 ms; circles, 10 s; squares, 40 s; triangles, ~300 s phase) observed at 0.6 M urea. The dotted symbols at 5 M urea represent time constants obtained from the unfolding double-jump assays. Conditions are described in the caption to Figure 1.

3, a second slow phase can be observed in this region as well if >20 kinetic traces are simultaneously fit to two exponentials (see below). The near equality of the two relaxation times and the small amplitude of the slower phase make the resolution of these two phases difficult. Although the time constant of the minor, slower unfolding phase has a higher uncertainty, a fully correlated error analysis suggests that it is considerably greater than any of the phases that have been previously observed for αTS in urea (*20*, *27*) or Gdn-HCl (*28*).

A key feature of the unfolding amplitudes (data not shown) is that there are two distinct regions where the fractional amplitude of the slow phase is nearly independent of final urea concentration. Between 2 and 3 M urea, approximately 25% of the amplitude is attributed to the slower phase. The amplitude of this phase then monotonically decreases to approximately 5−10% by 4 M urea and remains constant at higher urea concentrations. Consistent with previous observations, no burst phase is observed upon unfolding at any final urea concentration (Figure 1).

Refolding Kinetics to Varying Final Urea Concentrations (8 → x M Urea). The refolding of αTS exhibits multiphasic kinetics whose time constants display a complex dependence on final urea concentration. A representative kinetic trace, jumping from 6 to 0.6 M urea, is shown in Figure 2B. Under strongly refolding conditions (<1.2 M urea), the kinetics exhibit four observable phases: a fast kinetic phase of approximately 500 ms (inset) and three additional slower phases having time constants of approximately 10, 40, and ~300 s. The existence of four phases is inferred from the randomness of the residuals and the reduction in the reduced χ^2 upon inclusion of a fourth phase. The relative amplitudes of these phases are 5%, 55%, 30%, and 10%, respectively. Between 1.2 and 2.2 M urea, the 10 and 40 s phases were not readily distinguishable and, thus, appeared as a single kinetic phase with a time constant increasing from ~20 to ~70 s with increasing urea concentration (Figure 3). The time constant of the ~300 s phase does not depend strongly on the denaturant concentration. By contrast, the 500 ms phase accelerates sharply as the final urea concentration increases.

The refolding time constants and amplitudes did not depend on whether refolding was initiated from 5 or 8 M urea, where the I2 and U species, respectively, are the dominant states (G. Saab-Rincon, P. G. Gualfetti, O.B., and C.R.M., unpublished data). This result implies that I2 and U interconvert within the dead-time of mixing, 5 ms, under strongly folding conditions. The observable phases are preceded by a reaction that is complete within the dead-time of mixing and accounts for ~50% of the expected total ellipticity at 222 nm at 0.6 M urea. The amplitude of this burst phase decreases almost linearly with increasing urea concentration (Figure 1), demonstrating that the corresponding species has marginal stability. The observation that a burst-phase reaction accompanies the refolding of the I2 species implies that I2 is the precursor for the associated burst-phase intermediate.

Unfolding Kinetics from Varying Initial Urea Concentrations (x → 6 M Urea). The two phases detected in unfolding raise the question of whether the second phase originates from the formation of the I1 intermediate or from the presence of two native conformers for αTS. Because the amplitudes are directly proportional to the concentrations of the species present before unfolding (*36*), comparison of amplitudes obtained from varying initial conditions with those predicted from equilibrium studies permits a discrimination between these models.

The amplitudes of the unfolding phases recovered from the global fit of this data set are shown in Figure 4. Fits of these data to both a two-state and a three-state equilibrium denaturation model lead to the conclusion that the two-state fit is statistically more significant. The midpoints of the denaturation profiles are near or below 3 M, close to the midpoint of the N ⇄ I1 equilibrium transition (*20*). The absence of a transition corresponding to the unfolding of the I1 intermediate, with a midpoint near 3.8 M, supports the conclusion that the sequential model is incorrect. Therefore, the data strongly suggest that the unfolding of a minor nativelike species, in parallel with the dominant native form, gives rise to the slower unfolding reaction.

Refolding Double-Jump Assays (0 → 8 M → Delay → 0.4 M Urea). Double-jump refolding assays that test for the presence of slowly interconverting unfolded populations (*48*) were performed by monitoring the refolding kinetics as a function of delay time under unfolding conditions. Because these experiments were done by manual-mixing, the fastest (~500 ms) kinetic phase was not monitored. The recovered amplitudes of the three observable phases as a function of unfolding delay time are shown in Figure 5.

The amplitudes for all three refolding kinetic phases depend on the unfolding delay time, suggesting that multiple unfolded populations reequilibrate on the 10−100 s time scale. Because this redistribution is described by no fewer than three time constants, at least four unfolded populations must exist. A second significant feature is that the total

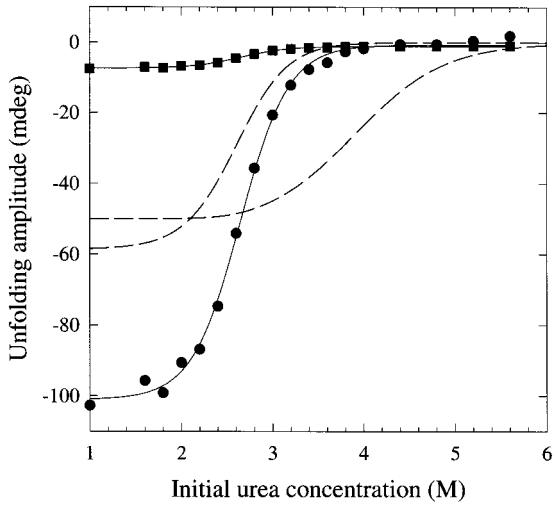

FIGURE 4: Unfolding from varying initial urea concentrations, represented as a superimposed plot of unfolding amplitudes at 6 M urea of both kinetic phases as a function of initial urea concentration. Symbols represent the amplitude of the fast unfolding (circles, $\tau = 13.7$ s) and the amplitude of the slow unfolding (squares, $\tau = 38$ s) phases, respectively. The solid lines represent a fit of the data to a two-state denaturation curve with $\Delta G° = 5.91 \pm 0.20$ kcal mol^{-1} and $m = 2.23 \pm 0.07$ kcal mol^{-1} M^{-1}. The native and unfolded baselines were taken to have zero slope because all of the data was collected under the same final conditions. The dashed lines represent amplitudes expected if the unfolding followed a sequential mechanism. Thermodynamic parameters from the three-state equilibrium fit to the data in Figure 1 (see Results) were used to calculate the simulated curves for the sequential mechanism. Conditions are described in the caption to Figure 1.

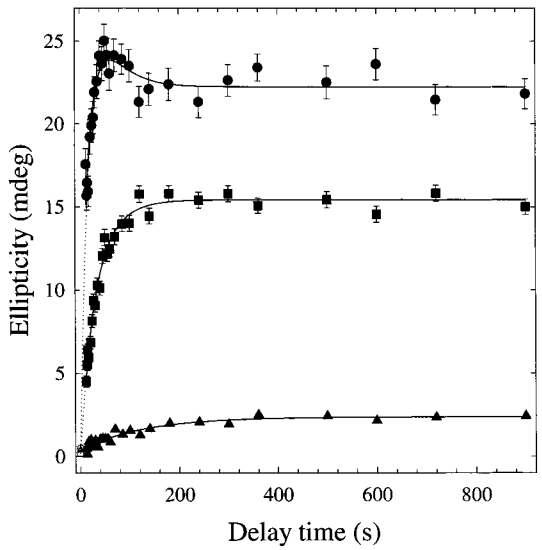

FIGURE 5: Double-jump refolding assay (0 M → 8 M → time delay → 0.4 M urea) showing the refolding amplitudes as a function of unfolding delay time. The symbols represent the unnormalized refolding amplitudes as recovered from a three-exponential fit: 10 s phase (circles), 40 s phase (squares), and ~300 s phase (triangles). The solid lines are a fit of these amplitudes to a constant plus three exponentials with linked time constants of $\tau_1 = 20 \pm 7$ s, $\tau_2 = 41 \pm 12$, and $\tau_3 = 124 \pm 25$ s. The extrapolated amplitudes at zero delay time are indicated by the dotted lines and corresponding open symbols. Conditions are as described in the caption of Figure 1.

predicted refolding amplitude extrapolated to zero time is only ~2−3% of the amplitude observed after complete equilibration. Because αTS completely unfolds in <10 s under these conditions, the missing amplitude implies that the initial unfolded form can refold substantially faster than

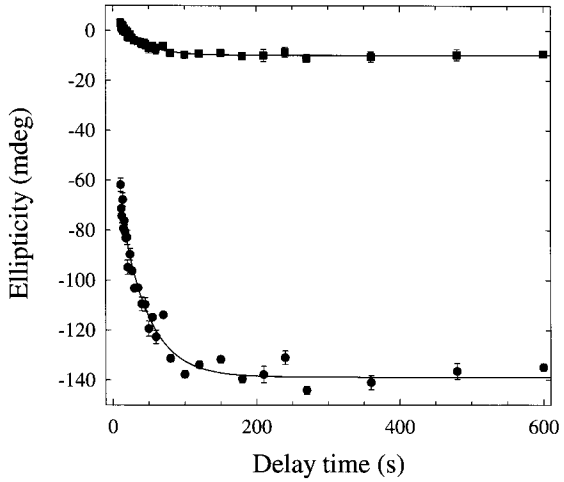

FIGURE 6: Double-jump unfolding assay (5 M → 0.25 M → time delay → 5 M urea) showing the fast (circles) and slow (squares) unfolding amplitudes as a function of refolding delay time. The amplitudes were obtained from a global fit of the unfolding traces as described in Materials and Methods. The solid lines represent a single-exponential fit with a time constant of 35 ± 4 s for the fast phase and 33 ± 3 s for the slow phase. Final protein concentration was 5 μM. Conditions are described in the caption to Figure 1.

the ~6−8 s dead-time of the refolding jump. The dramatic increase in refolding amplitudes with increasing unfolding delay time indicates that this initial unfolded state is only marginally (≤5%) populated under equilibrium unfolding conditions.

Unfolding Double-Jump Assays (5 → 0.25 M → Delay → 5 M Urea). Unfolding double-jump assays can be used to probe the native state population at various refolding times (*49*). This technique exploits the fact that unfolding from the native state is expected to be considerably slower than unfolding from marginally stable intermediates. The recovered unfolding amplitudes for αTS as a function of refolding delay time at 0.25 M urea are presented in Figure 6.

A statistically significant burst phase ($\tau \leq 10$ s) comprising ~50% of the total unfolding amplitude is observed for the dominant native form. This suggests that the slower refolding phases are not rate-limiting in the formation of native αTS at 0.25 M urea. By contrast, no significant burst phase is observed for the minor unfolding reaction. Following the rapid appearance of signal, the remaining unfolding amplitude is recovered on a time scale of 34 ± 4 s for both unfolding phases. The unfolding double-jump assays therefore indicate that the recovery of the dominant native species is multiphasic, with one or more kinetic phases having $\tau \leq 10$ s and another with $\tau = 34$ s.

Unfolding Double-Jump Assays (5 → 0.25 M → Delay → 2.4 M Urea). To probe the interconversion of transiently populated high energy native and possible multiple I1 conformers, unfolding double-jump assays to 2.4 M urea were performed. At this urea concentration, this assay probes the transfer of only a fraction (~25%) of the native species to the I1 equilibrium intermediate state(s).

Kinetics traces reflecting unfolding to 2.4 M urea after various refolding delay periods at 0.25 M urea are shown in Figure 7. A striking feature of these data is the systematic manner in which the amplitudes of *both* phases change sign between the earliest delay time (30 s, panel A) and longest delay time (900 s, panel D). The nonmonotonic response in

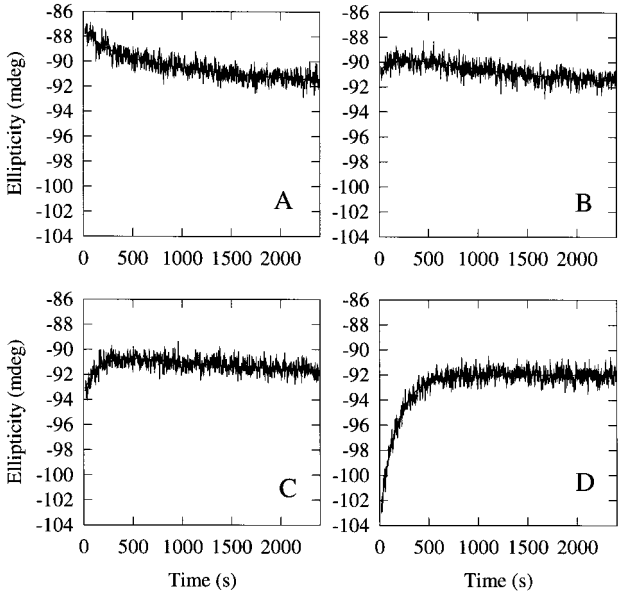

FIGURE 7: Double-jump unfolding assay (5 M → 0.25 M → time delay → 2.4 M urea) showing the kinetic traces at refolding delay times of (A) 30 s, (B) 45 s, (C) 90 s, and (D) 900 s. Lines represent global fits of the unfolding traces to two exponentials with linked time constants of 167 ± 15 and 1322 ± 400 s. Final protein concentration was 1.8 μM. Conditions are described in the caption to Figure 1.

Figure 7B,C shows that the amplitudes do not change sign in a concerted fashion. The positive amplitudes at early delay times indicate that the population of N is less than its equilibrium population at 2.4 M urea. At longer delay times, a significant population of N is achieved and jumps to 2.4 M urea result in a decrease in ellipticity that reflects net unfolding.

Refolding Kinetics from Varying Initial Urea Concentrations (x → 0.6 M Urea). The presence of an equilibrium intermediate for αTS near 3 M urea permits a test of its relationship to the intermediates detected in kinetic studies. The refolding amplitudes from various initial urea concentrations were obtained from a global fit of the associated data set and are shown in Figure 8. Although the amplitude of the 40 s phase increases in a simple sigmoidal fashion, the ~300 s and possibly the 10 s phases display inflections that are indicative of three participating species. Fits of these data to two- or three-state models reveal that all three amplitudes have a midpoint which corresponds closely to the N ⇄ I1 equilibrium transition. Only the amplitudes of the 10 and ~300 s phases have a second midpoint that is very similar to that for the I1 ⇄ I2/U transition. The validity of the fit of the 10 s amplitude data to a three-state model is supported by a statistical analysis and by consideration of the equilibrium unfolding model.

Elucidation of a Kinetic Model. The data presented above define many of the basic features of the kinetic folding mechanism for αTS. For example, consideration of the double-jump refolding assays, unfolding assays, and refolding/unfolding kinetics from different initial conditions gives strong support for the existence of at least four unfolded states and two nativelike states. Although the presence of multiple intermediate states can also be inferred from these results, more direct evidence comes from two pieces of data: the observation that at least one of the native states is

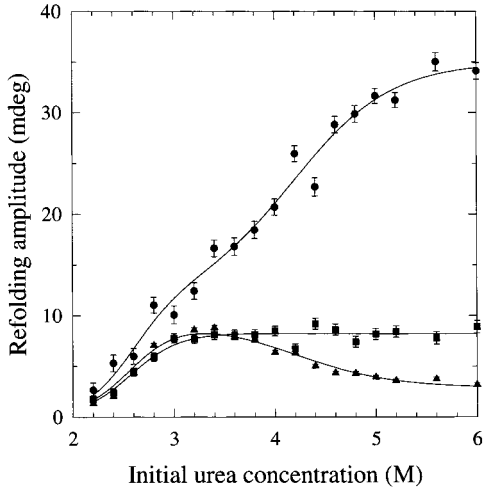

FIGURE 8: Refolding to 0.6 M urea from varying initial urea concentrations. The refolding amplitudes of the 10 s (circles), 40 s (squares), and ~300 s (triangles) phases are shown superimposed as a function of initial urea concentration.The solid lines represent fits to a three-state denaturation model in which the free energies and *m*-values are linked. The values obtained from the fit are the following: $\Delta G_{NI} = 7.9 \pm 2.0$ kcal (mol)$^{-1}$; $m_{NI} = 2.9 \pm 0.5$ kcal (mol)$^{-1}$ (molar urea)$^{-1}$; $\Delta G_{IU} = 5.4 \pm 1.0$ kcal (mol)$^{-1}$; $m_{IU} = 1.3 \pm 0.2$ kcal (mol)$^{-1}$ (molar urea)$^{-1}$. Conditions are described in the caption to Figure 1.

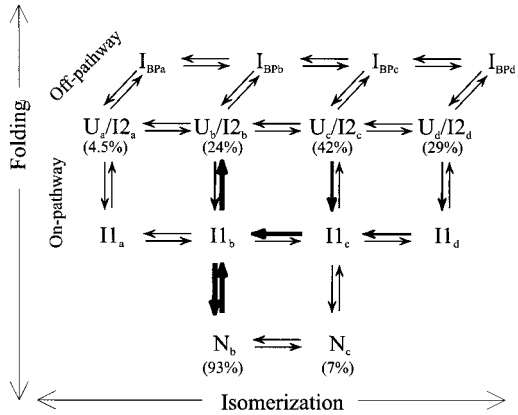

FIGURE 9: Kinetic folding model for αTS. Folding reactions are depicted as proceeding along the vertical direction and isomerization reactions proceed along the horizontal direction. The vertical direction is further subdivided into on- and off-pathway intermediates. The numbers in parentheses represent the equilibrium populations of the unfolded and native forms. The thickest arrows represent the major pathways for folding and unfolding. In refolding, channels c and d carry the majority of the population. Unfolding proceeds mainly from the dominant native form, N_b, and through channel b.

populated in a multiphasic manner (Figure 6) and the finding of a complex urea dependence of the amplitudes in the *x* → 0.6 M jumps (Figure 8).

A kinetic model that satisfies all of the constraints imposed by the data is shown in Figure 9. This model, which has features similar to several proposed previously (*27*, *50*), postulates that four unfolded ensembles, U_a−U_d, serve as the starting point of four refolding channels. The spectroscopic similarity of U and I2 and the inability to distinguish between them in kinetic experiments dictates that these species be considered as a single entity in the model. In effect, this assumption implies that I2 and U are in rapid equilibrium on the millisecond time scale under strongly folding conditions. Within 5 ms, a set of off-pathway burst-phase intermediates, I_{BPa}−I_{BPd}, are populated. Over the next

Table 1: Microscopic Rate Constants and Kinetic $m^{\ddagger}$ Values Obtained from the Global Fit to the Proposed Folding Mechanism for αTS[a]

reaction	$k_{forward}$ (→) (s^{-1})	$m^{\ddagger}_{forward}$ (→) (kcal mol^{-1} M^{-1})	$k_{reverse}$ (←) (s^{-1})	$m^{\ddagger}_{reverse}$ (←) (kcal mol^{-1} M^{-1})
$U/I2_{a-d} \rightleftarrows I_{BPa-d}$	540[b]	0[b]	3.50 (0.21)[b]	−1.01 (0.01)[b]
$U/I2_{a-d} \rightleftarrows I1_{a-d}$	100[b]	0[b]	0.051 (0.002)[c]	−1.23 (0.01)[c]
$I1_b \rightleftarrows N_b$	11.3 (0.3)	1.47 (0.01)	3.0×10^{-4} (0.02×10^{-4})	−0.52 (0.01)
$I1_c \rightleftarrows N_c$	0.18 (0.01)	1.78 (0.08)	0.9×10^{-4} (0.5×10^{-5})	−0.60 (0.01)
$U/I2_a \rightleftarrows U/I2_b$	0.019[d]	0[e]	3.6×10^{-3} [d]	0[e]
$U/I2_b \rightleftarrows U/I2_c$	7.7×10^{-3} [d]	0[e]	4.4×10^{-3} [d]	0[e]
$U/I2_c \rightleftarrows U/I2_d$	0.019[d]	0[e]	0.028[d]	0[e]
$I1_a \rightleftarrows I1_b$	6.4×10^{-3} (0.07×10^{-3})	0[e]	0.018 (0.0006)	0[e]
$I1_b \rightleftarrows I1_c$	0.20 (0.01)	0[e]	0.12 (0.002)	0[e]
$I1_c \rightleftarrows I1_d$	4.0×10^{-3} (0.03×10^{-3})	0[e]	0.072 (0.005)	0[e]

[a] Values in parentheses represent the standard deviation obtained from an uncorrelated error analysis of the fit. The absence of parentheses denotes a fixed parameter. The optical properties of the native and unfolded species are indicated by the dotted baselines in Figure 1 and were held fixed during the fitting. The optimized *Z*-values of the burst-phase and I1 intermediates were 0.37 and 0.57, respectively. [b] This phase occurs within the burst phase of the stopped-flow reaction; therefore, independent information on the forward and reverse reactions is not available. The forward rate was specified to give rise to a completed reaction within the earliest observable times (∼5 ms). The reverse reaction was allowed to vary and to carry the urea dependence of the burst-phase species. [c] The reverse reaction indicated corresponds to that for channel b. The reverse rates for the other channels are comparable and were determined by considering the thermodynamic cycle. For example, the reverse rate for channel a is calculated using the expression $\Delta G^{\circ}_{U/I2a-I1a} + \Delta G^{\circ}_{I1a-I1b} + \Delta G^{\circ}_{I1b-U/I2b} + \Delta G^{\circ}_{U/I2b-U/I2a} = 0$ and recognizing that $\Delta G^{\circ}_{U/I2a-I1a} = -RT \ln((k_{U/I2a-I1a})/(k_{I1a-U/I2a}))$. Although all of the urea dependence was assigned to the reverse reaction, this arbitrary assignment does not affect the analysis because only the equilibrium properties of the U/I2 ⇄ I1 reaction contribute to the mechanism. Neither the forward nor the reverse steps are directly obtained in these experiments. [d] These values were calculated from the time constants and amplitudes of the double-jump refolding assay (Figure 5). [e] Isomerization reactions were assumed to have urea-independent rates.

several hundred milliseconds, a set of intermediates, $I1_a$−$I1_d$, appear. The formation of these species is limited by the unfolding of I_{BPa}−I_{BPd}, thus accounting for the decrease in the time constant at higher urea concentration (Figure 3). $I1_a$−$I1_d$ correspond to the equilibrium intermediate detected at 3 M urea, I1. On the basis of the refolding double-jump assays, the minor channel (b) directly leads to formation of the more stable native species, N_b, in several hundred milliseconds. The intermediates in the a, c, and d channels, which together represent the majority of the population, require relatively slow (>10 s) isomerization/rearrangement reactions before reaching the native state. Under marginal folding conditions, e.g., 2 M urea, the strong urea dependence of the $I1_b \rightarrow N_b$ reaction makes it the rate-limiting step in folding. The rate-limiting unfolding reactions are $N_b \rightarrow I1_b$ and $N_c \rightarrow I1_c$. The interconversion rate between the two native species must be slow (>1000 s) on the experimental time scale to account for the observation of two kinetic phases and the very slow recovery of the amplitudes shown in Figure 7.

Each of the individual species in this kinetic model is presumed to represent ensembles of rapidly interconverting forms. The acquisition of secondary structure implies that the size of these ensembles, however, dramatically decreases as the reaction proceeds from unfolded to intermediate to native conformers.

The direct interconversion between the a and d channels for the intermediate and unfolded species is a formal possibility. However, the observation that the recovery of the ∼250 s refolding phase in the double-jump refolding assay is well-described by a single slow exponential suggests that there is no rapid interconversion between the a and d channels. Therefore, the present model is deemed a reasonable approximation to the kinetic and equilibrium folding properties of αTS.

Global Analysis of Kinetics. A global analysis of a subset of the kinetic data was performed to test further the model presented in Figure 9 and to obtain quantitative estimates of the microscopic rate constants and the corresponding kinetic

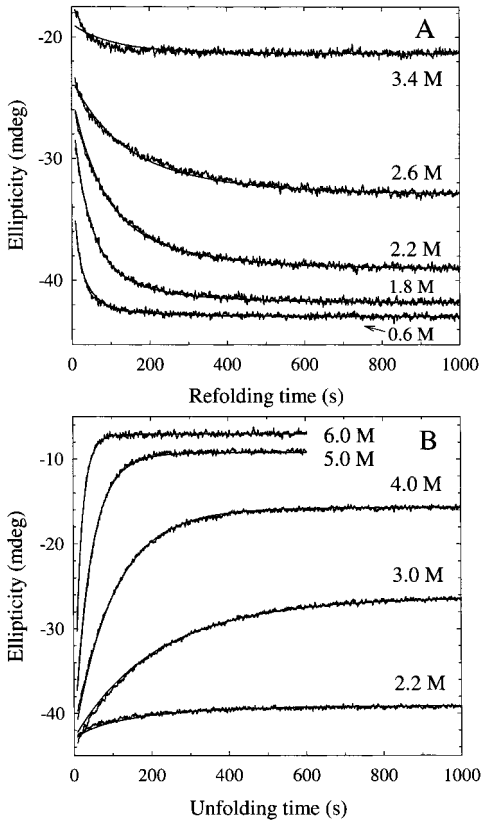

FIGURE 10: Refolding (A) and unfolding (B) manual-mixing CD kinetic traces at representative urea concentrations with superimposed global fits to model shown in Figure 9 (lines). The complete data set was comprised of 113 kinetic traces. The kinetic traces have been normalized to a protein concentration of 1 μM.

$m^{\ddagger}$ values (Table 1). A total of 113 kinetic traces, including 59 unfolding jumps (0 → *x* M urea) and 54 refolding jumps (either 6 → *x* or 8 → *x* M urea) were included in the global fit. The results are presented in Figure 10. The kinetic model gives good quantitative agreement with both the refolding and unfolding kinetic data with the exception of the region near 3 M urea. The discrepancies where I1 is highly populated may reflect the assumption that the interconversion

rates between the I1 conformers are independent of denaturant concentration. The possibility of this discrepancy arising from the use of a linear baseline for the unfolded form (*51*) was tested by inclusion of a nonlinear term for the unfolded baseline. However, this modification did not yield statistically significant improvements in the fit. Alternatively, the actual folding model may be more complex in the transition region. A corresponding simulation of the equilibrium denaturation curve based solely on the kinetic data is shown in Figure 1. The excellent agreement between this simulation and the equilibrium model further supports the choice of the model.

The time constants at a given urea concentration, which can be obtained from diagonalization of the rate matrix (eq 1), are compared to the experimental values in Figure 3. The good agreement between observed and calculated time constants lends further support to the model. The four relaxation times predicted between 1 and 4 M urea in the hundreds of milliseconds time range represent the behavior of the four burst phase intermediates, $I_{BPa}-I_{BPd}$. Minor differences between the four predicted relaxation times represents differential coupling between the burst phase unfolding reaction and subsequent steps in the folding reaction. Throughout the entire urea concentration range, however, there are regions where the calculated time constants are not observed in the single-jump experiments. Kinetic phases that arise primarily from isomerization reactions among native, intermediate, or unfolded forms are observed only under conditions where they are rate-limiting. For example, the three longest time constants at 8 M urea are only observed in the refolding double-jump experiment (Figure 5). Another example is provided by the absence of a ~5000 s time constant at 1 M urea. This phase represents the interconversion of the two native conformers which are presumed to be spectroscopically similar. In addition, this analysis also demonstrates that the correspondence between the experimental time constants and the microscopic rate constants in a kinetic model can be complex.

The relative free energy for each of the species in the kinetic model at 0, 3, and 6 M urea is shown in Figure 11. The relative population of the set of burst-phase intermediates is dictated by that of the unfolded state because folding to I_{BP} is far faster than interconversion among the U conformers. The average stability of I_{BP}, ≤ 3 kcal mol^{-1}, was estimated by considering that it is formed from I2/U within 5 ms and unfolds in the hundreds of milliseconds time range between 0.6 and 3.5 M urea (Figure 3). The similar free energies and, by inference, the populations of multiple conformers in each of the N, I1, and I2/U states illustrate the underlying complexity of the equilibrium folding model.

No attempt was made to estimate the activation free energies for the transition states in the unfolding and refolding reactions for αTS. Uncertainties in the value of the preexponential factor relating rate constants and activation free energies make such calculations ambiguous.

DISCUSSION

The combination of a variety of folding/unfolding assays together with a global analysis has yielded new insights into the folding mechanism of αTS. First, four kinetically distinguishable unfolded forms of αTS give rise to parallel folding channels. Interchannel isomerization reactions only become competitive with intrachannel folding reactions at a late stage in the process. Second, the earliest detectable folding reaction leads to an off-pathway, marginally stable intermediate. Models incorporating an on-pathway species were not capable of fitting the data. Third, the formation of the principal native species can occur in the hundreds of milliseconds time range. This time scale is surprisingly short for a large protein that folds through several intermediates. Fourth, the equilibrium intermediate detected at 3 M urea also appears transiently during the folding reaction. The kinetic studies reveal, however, that this equilibrium species is actually comprised of four similar but slowly interconverting forms. Finally, the native state of αTS is composed of two slowly interconverting conformers. The isomerization reaction that links these native species appears to be identical to that which distinguishes a pair of unfolded conformers.

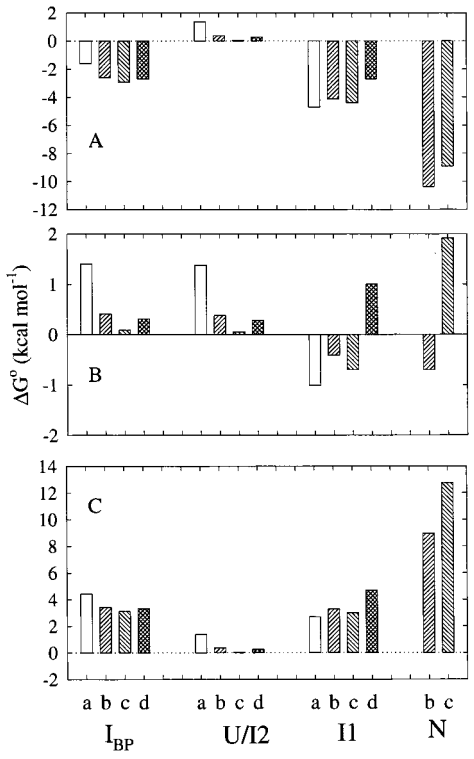

FIGURE 11: Free energy diagrams showing the relative free energies of the kinetic species at 0 M (A), 3 M (B), and 6 M urea (C). The free energies were calculated using the microscopic rate constants shown in Table 1. The free energies were normalized to the free-energy of the unfolded state of channel C ($I2/U_c$) plus an arbitrary offset, 0.05 kcal mol^{-1}, to simplify visualization of this state in the bar graph.

Origin of the Parallel Channels. The double-jump refolding assays and the single-jump unfolding data give strong support for the presence of multiple ensembles in the urea-denatured unfolded states of αTS. One possible explanation for slowly interconverting unfolded forms is provided by cis/trans isomerization about Xaa−Pro peptide bonds (*48*, *52*). Of the 19 prolyl residues in αTS, only Pro 28 is in the cis isomeric form in the native conformation (D. R. Davies, personal communication). The prediction that the dominant unfolded form folds to the minor native conformer (Figure 9) suggests Pro 28 may be responsible for the pair of native conformers and two of the unfolded conformers.

Yutani and his colleagues have replaced six conserved prolines, including Pro 28, with alanine and detected two

slow refolding phases that were very similar to those detected in wild-type αTS (*53*). These results suggest that if Pro 28 does play a role in the slow folding kinetics, it must involve one of the faster isomerization reactions, e.g., the $I1_c \rightarrow I1_b$ reaction. This conjecture is consistent with the loss of the minor slow unfolding phase for P28A (*53*). Other candidates include Pro 93, which is known to form about 5% of the cis isomer in the urea-unfolded form (*21*), and Pro 96 and Pro 207, which, when replaced by alanine, display only a single unfolding phase (*53*).

Parallel channel folding models involving proline isomerization have been postulated for staphylococcal nuclease (*54*, *55*), ribonuclease A (*56*−*59*), thioredoxin (*60*, *61*), and ribonuclease T1 (*49*, *62*). The 10−1000 s time constants typical of cis/trans proline isomerization reactions are apparently slower than accessible folding reactions, leading to the development of parallel folding channels in these proteins. Reequilibration among late intermediates or native conformers allows the system to reach a minimum in free energy. Proline isomerization has also been demonstrated to be responsible for the multiple slowly interconverting native conformers in staphylococcal nuclease (*63*) and calbindin D9k (*64*).

Early Intermediates in the Refolding of αTS. The earliest observed refolding intermediates, I_{BP}, of αTS are characterized by marginal stability (≤3 kcal mol^{-1}), significant secondary structure, and the formation of hydrophobic surface (J.A.Z. and C.R.M., unpublished result). Similar properties were observed for the burst-phase intermediate recovered from Gdn-HCl denaturation (*28*), leading to the suggestion that the burst-phase intermediate is a molten globule (*6*). This species was also proposed to correspond to the Gdn-HCl stabilized equilibrium intermediate that is equivalent to the I1 species populated at 3 M urea (*65*). Although several optical properties (e.g., CD and fluorescence) of the burst-phase species are similar to those of I1, these intermediates are not likely to be identical. The most compelling evidence is the absence of a sigmoidal burst-phase denaturation profile which overlaps that for the unfolding of the equilibrium I1 intermediate (Figure 1). Further support for this conclusion is provided by the finding that the subsequent set of kinetic intermediates, $I1_a$−$I1_d$, does have the requisite stability and optical properties.

It is possible that the burst-phase species recovered by rapid dilution of urea-denatured αTS is not that observed by dilution of Gdn-HCl-denatured protein. The absence of a refolding phase in the 100 ms time range in the Gdn-HCl studies (*28*) suggests that folding may proceed directly to the set of I1 intermediates. The greater potency of Gdn-HCl as a denaturant may prevent the formation of the marginally stable off-pathway intermediate detected when refolding from urea.

The presence of both off and on-pathway intermediates for αTS may reflect the known propensity of amino- and carboxy-terminal fragments to fold in isolation (*66*). Residues 1−188 adopt secondary structure with significant stability, and residues 189−268 adopt secondary structure; however, the stability is marginal (*67*). The independent formation of organized structure offers the possibility that these domains or even smaller subdomains may associate to form either nativelike or nonnativelike complexes. Nonnative complexes would have to unfold before proceeding down a productive pathway. Nativelike complexes, by contrast, would be competent to fold directly to the native conformation. Another possibility is that the off-pathway species represents a rapid collapse that is driven by the formation of local elements of secondary structure that are loosely associated. The on-pathway species would represent coalescence of autonomously folding domains into a direct precursor to the native conformation. The dominance of the off-pathway form at the earliest stage of folding indicates that its rate of formation exceeds that of the more stable on-pathway intermediate.

Rate-Limiting Steps in the Folding/Unfolding of αTS. The development of a quantitative kinetic model for αTS leads to insights into the magnitude and nature of the barriers in the folding/unfolding reactions. The rate-limiting steps in the unfolding of αTS are the conversion of $N_b \rightarrow I1_b$ and $N_c \rightarrow I1_c$ along independent, parallel channels. This interpretation assumes that the interconversion rate between the pair of native species is considerably slower than the unfolding rate at denaturant concentrations above 1.5 M urea. This assumption is supported by the double-jump unfolding assays that demonstrate multiple slow time scales for the formation of the respective nativelike species (Figures 6 and 7).

The finding that the unfolding of each of the native forms of αTS proceeds in a two-state manner with similar rates (2.95×10^{-4} and 0.895×10^{-4} s^{-1} for $k_{Nb \rightarrow I1b}$ and $k_{Nc \rightarrow I1c}$, respectively) suggests that structures and energies of the corresponding transition state ensembles must also be similar. This conjecture is supported by the near equivalence of the denaturant dependence of both the refolding and unfolding rates, i.e., the $m^{\ddagger}$ values and the position of the transition state along the reaction coordinate, as quantified by $\alpha = m_f^{\ddagger}/(m_f^{\ddagger} - m_u^{\ddagger})$ (*68*); α is near 0.75 for both the b and c channels. Mutagenesis studies comparing the perturbations of the unfolding and refolding rate constants for the N1 ⇄ I1 reaction indicate that the transition state ensemble has nativelike side-chain packing, unlike the intermediate state (*69*). Therefore, although the relative free energies of the two native conformers differ by 2 kcal mol^{-1}, the structural and energy differences between them must persist in the corresponding transition state ensembles. The assignment of the difference between the native conformers to a proline isomerization reaction is consistent with this conclusion.

The observation that very similar unfolding transition states are accessed by native conformers of significantly different stabilities implies that no other transition states within 2 kcal mol^{-1} exist for αTS. By contrast, barstar can unfold through either of two structurally different transition states depending on the solution conditions (*70*). The difference between αTS and barstar may reflect the significant stability of the I1 intermediates for αTS and the nativelike transition states that link the N and I1 manifolds. In the absence of species with these properties, multiple saddle points on the energy surface could have comparable energies.

Under strongly folding conditions, the refolding step with the highest free-energy barrier along each of the channels involves the reverse reactions, $I1_x \rightarrow N_x$ (Figure 9). For the dominant folding channel, the rate constant for $I1_b \rightarrow N_b$ is ∼100 ms in the absence of denaturant. This rate is over 1 order of magnitude faster than the channel leading to the minor native conformer and the isomerization steps between any two channels in the kinetic model. At 1.5 M urea,

however, this rate-limiting step becomes comparable to the interchannel isomerization rates. Above 2.0 M urea, $I1_b \rightarrow N_b$ is the rate-limiting step in the folding of αTS. This behavior is consistent with the absence of a burst-phase amplitude, i.e., for $\tau < 10$ s, in double-jump unfolding assays delaying at >1 M urea (data not shown).

General Implications for the Folding Mechanisms of Large Proteins. The global analysis of the folding mechanism for αTS demonstrates that microscopic rate constants for individual steps can be obtained, even in a system with parallel channels and multiple transient intermediates. This approach opens the way for the thermodynamic and mutational analysis of the energetics and structures of the partially folded forms that often appear during the folding of large proteins (>100 amino acids). In combination with insights into transition states available from mutational and other studies, it may be possible to construct an energy surface for the entire folding reaction. Comparisons of such experimental information with theoretical predictions (*71*, *72*) may eventually lead to algorithms for predicting folding pathways of proteins.

ACKNOWLEDGMENT

The authors acknowledge Drs. Xiaowu Chen, Gloria Saab-Rincón, and Peter J. Gualfetti for their early contributions to this work. We also thank Drs. Patricia Jennings, Ramakrishna Vadrevu, Virginia Smith, and Roxana Ionescu for helpful discussions.

REFERENCES

1. Kim, P. S., and Baldwin, R. L. (1982) *Annu. Rev. Biochem. 51*, 459−489.
2. Kim, P. S., and Baldwin, R. L. (1990) *Annu. Rev. Biochem. 59*, 631−660.
3. Matthews, C. R. (1993) *Annu. Rev. Biochem. 62*, 653−683.
4. Roder, H., and Colon, W. (1997) *Curr. Opin. Struct. Biol. 7*, 15−28.
5. Kuwajima, K. (1989) *Proteins 6*, 87−103.
6. Ptitsyn, O. B. (1995) *Adv. Prot. Chem. 47*, 83−229.
7. Jennings, P. A., and Wright, P. E. (1993) *Science 262*, 892−896.
8. Arai, M., and Kuwajima, K. (1996) *Folding Des. 1*, 275−287.
9. Raschke, T. M., and Marqusee, S. (1997) *Nat. Struct. Biol. 4*, 298−304.
10. Bai, Y., Sosnick, T. R., Mayne, L., and Englander, S. W. (1995) *Science 269*, 192−197.
11. Bai, Y., and Englander, S. W. (1996) *Proteins 24*, 145−156.
12. Englander, S. W., Mayne, L., Bai, Y., and Sosnick, T. R. (1997) *Protein Sci. 6*, 1101−1109.
13. Chamberlain, A. K., and Marqusee, S. (1998) *Biochemistry 37*, 1736−1742.
14. Oas, T. G., and Kim, P. S. (1988) *Nature 336*, 42−48.
15. Chaffotte, A. F., Cadieux, C., Guillou, Y., and Goldberg, M. E. (1992) *Biochemistry 31*, 4303−4308.
16. Tasayco, M. L., and Carey, J. (1992) *Science 255*, 594−597.
17. Dobson, C. M., Evans, P. A., and Radford, S. E. (1994) *Trends Biochem. Sci. 19*, 31−37.
18. Radford, S. E., and Dobson, C. M. (1995) *Philos. Trans. R. Soc. London B. Biol. Sci. 348*, 17−25.
19. Farber, G. K., and Petsko, G. A. (1990) *Trends Biochem. Sci. 15*, 228−234.
20. Matthews, C. R., and Crisanti, M. M. (1981) *Biochemistry 20*, 784−792.
21. Saab-Rincon, G., Froebe, C. L., and Matthews, C. R. (1993) *Biochemistry 32*, 13981−13990.
22. Eder, J., and Kirschner, K. (1992) *Biochemistry 31*, 3617−3625.
23. Jasanoff, A., Davis, B., and Fersht, A. R. (1994) *Biochemistry 33*, 6350−6355.
24. Sanchez del Pino, M. M., and Fersht, A. R. (1997) *Biochemistry 36*, 5560−5565.
25. Crisanti, M. M., and Matthews, C. R. (1981) *Biochemistry 20*, 2700−2706.
26. Beasty, A. M., and Matthews, C. R. (1985) *Biochemistry 24*, 3547−3553.
27. Tweedy, N. B., Hurle, M. R., Chrunyk, B. A., and Matthews, C. R. (1990) *Biochemistry 29*, 1539−1545.
28. Ogasahara, K., and Yutani, K. (1994) *J. Mol. Biol. 236*, 1227−1240.
29. Choi, S.-G., and Hardman, J. K. (1995) *J. Biol. Chem. 270*, 28177−28182.
30. Kirschner, K., Wiskocil, R. L., Loehn, M., and Rezeau, L. (1975) *Eur. J. Biochem. 60*, 513−523.
31. Matthews, C. R., Crisanti, M. M., Manz, J. T., and Gepner, G. L. (1983) *Biochemistry 22*, 1445−1452.
32. Mann, C. J., and Matthews, C. R. (1993) *Biochemistry 32*, 5282−5290.
33. Pace, C. N., Shirley, B. A., and Thomson, J. A. (1989) in *Protein structure: A practical approach* (Creighton, T. E., Ed.) pp 311−330, IRL Press, Oxford, U.K.
34. Finn, B. E., Chen, X., Jennings, P. A., Saalau-Bethell, S. M., and Matthews, C. R. (1992) in *Protein Engineering: A Practical Approach* (Rees, A. R., Sternberg, M. J. E., and Wetzel, R., Eds.) pp 167−189, IRL Press, Oxford, U.K.
35. Schellman, J. A. (1978) *Biopolymers 17*, 1305−1322.
36. Tanford, C. (1968) *Adv. Prot. Chem. 23*, 122−282.
37. Knutson, J. R., Beechem, J. M., and Brand, L. (1983) *Chem. Phys. Lett. 10*, 501−507.
38. Zitzewitz, J. A., Bilsel, O., Luo, J., Jones, B. E., and Matthews, C. R. (1995) *Biochemistry 34*, 12812−12819.
39. Ikai, A., and Tanford, C. (1973) *J. Mol. Biol. 73*, 145−163.
40. Matthews, C. R. (1987) *Methods Enzymol. 154*, 498−511.
41. Marquardt, D. W. (1963) *J. Soc. Ind. Appl. Math. 11*, 431−441.
42. Henry, E. R., and Hofrichter, J. (1992) *Methods Enzymol. 210*, 129−192.
43. Hofrichter, J., Henry, E. R., Sommer, J. H., Deutsch, R., Ikeda-Saito, M., Yonetani, T., and Eaton, W. A. (1985) *Biochemistry 24*, 2667−2679.
44. McPhie, P., and Shrager, R. I. (1992) *Arch. Biochem. Biophys. 293*, 46−53.
45. Milder, S. J., Thorgeirsson, T. E., Miercke, L. J. W., Stroud, R. M., and Kliger, D. S. (1991) *Biochemistry 30*, 1751−1761.
46. Segel, D. J., Fink, A. L., Hodgson, K. O., and Doniach, S. (1998) *Biochemistry 37*, 12443−51.
47. Farooq, A. (1998) *Biochemistry 37*, 15170−15176.
48. Brandts, J. F., Halvorson, H. R., and Brennan, M. (1975) *Biochemistry 14*, 4953−4963.
49. Kiefhaber, T., Quaas, R., Hahn, U., and Schmid, F. X. (1990) *Biochemistry 29*, 3053−3061.
50. Hurle, M. R., and Matthews, C. R. (1987) *Biochim. Biophys. Acta 913*, 179−184.
51. Qi, P. X., Sosnick, T. R., and Englander, S. W. (1998) *Nat. Struct. Biol. 5*, 882−884.
52. Schmid, F. X., Mayr, L. M., Mucke, M., and Schonbrunner, E. R. (1993) *Adv. Prot. Chem. 44*, 25−66.
53. Ogasahara, K., and Yutani, K. (1997) *Biochemistry 36*, 932−940.
54. Kuwajima, K., Okayama, N., Yamamoto, K., Ishihara, T., and Sugai, S. (1991) *FEBS Lett. 290*, 135−138.
55. Ikura, T., Tsurupa, G. P., and Kuwajima, K. (1997) *Biochemistry 36*, 6529−6538.
56. Schultz, D. A., Schmid, F. X., and Baldwin, R. L. (1992) *Protein Sci. 1*, 917−924.
57. Dodge, R. W., and Scheraga, H. A. (1996) *Biochemistry 35*, 1548−1559.
58. Houry, W. A., and Scheraga, H. A. (1996) *Biochemistry 35*, 11719−11733.
59. Juminaga, D., Wedemeyer, W. J., and Scheraga, H. A. (1998) *Biochemistry 37*, 11614−11620.

60. Kelley, R. F., and Richards, F. M. (1987) *Biochemistry 26*, 6765−6774.
61. Georgescu, R. E., Li, J.-H., Goldberg, M. E., Tasayco, M. L., and Chaffotte, A. F. (1998) *Biochemistry 37*, 10286−10297.
62. Kiefhaber, T., Grunert, H. P., Hahn, U., and Schmid, F. X. (1990) *Biochemistry 29*, 6475−6480.
63. Alexandrescu, A. T., Hinck, A. P., and Markley, J. L. (1990) *Biochemistry 29*, 4516−4525.
64. Chazin, W. J., Kordel, J., Drakenberg, T., Thulin, E., Grundstrom, T., and Forsen, S. (1989) *Proc. Natl. Acad. Sci. U.S.A. 86*, 2195−2198.
65. Ogasahara, K., Matsuhita, E., and Yutani, K. (1993) *J. Mol. Biol. 234*, 1197−1206.
66. Higgins, W., Fairwell, T., and Miles, E. W. (1979) *Biochemistry 18*, 4827−4835.
67. Miles, E. W., Yutani, K., and Ogasahara, K. (1982) *Biochemistry 21*, 2586−2592.
68. Myers, J. K., Pace, C. N., and Scholtz, J. M. (1995) *Protein Sci. 4*, 2138−2148.
69. Tsuji, T., Chrunyk, B. A., Chen, X., and Matthews, C. R. (1993) *Biochemistry 32*, 5566−5575.
70. Zaidi, F., Nath, U., and Udgaonkar, J. B. (1997) *Nat. Struct. Biol. 4*, 1016−1023.
71. Daggett, V., Li, A., Itzhaki, L. S., Otzen, D. E., and Fersht, A. R. (1996) *J. Mol. Biol. 257*, 430−440.
72. Ladurner, A. G., Itzhaki, L. S., Daggett, V., and Fersht, A. R. (1998) *Proc. Natl. Acad. Sci. U.S.A. 95*, 8473−8478.

BI982365Q